Southern Ocean fronts: Controlled by wind or topography?

Robert M. Graham,[1,2,3] Agatha M. de Boer,[2,4] Karen J. Heywood,[1] Mark R. Chapman,[1] and David P. Stevens[5]

Received 11 January 2012; revised 31 May 2012; accepted 5 July 2012; published 17 August 2012.

[1] The location of fronts has a direct influence on both the physical and biological processes in the Southern Ocean. Here we explore the relative importance of bottom topography and winds for the location of Southern Ocean fronts, using 100 years of a control and climate change simulation from the high resolution coupled climate model HiGEM. Topography has primary control on the number and intensity of fronts at each longitude. However, there is no strong relationship between the position or spacing of jets and underlying topographic gradients because of the effects of upstream and downstream topography. The Southern Hemisphere Westerlies intensify and shift south by 1.3° in the climate change simulation, but there is no comparable meridional displacement of the Antarctic Circumpolar Current's (ACC) path or the fronts within its boundaries, even over flat topography. Instead, the current contracts meridionally and weakens. North of the ACC, the Subtropical Front (STF) shifts south gradually, even over steep topographic ridges. We suggest the STF reacts more strongly to the wind shift because it is strongly surface intensified. In contrast, fronts within the ACC are more barotropic and are therefore more sensitive to the underlying topography. An assessment of different methods for identifying jets reveals that maxima of gradients in the sea surface height field are the most reliable. Approximating the position of fronts using sea surface temperature gradients is ineffective at high latitudes while using sea surface height contours can give misleading results when studying the temporal variability of front locations.

Citation: Graham, R. M., A. M. de Boer, K. J. Heywood, M. R. Chapman, and D. P. Stevens (2012), Southern Ocean fronts: Controlled by wind or topography?, *J. Geophys. Res.*, *117*, C08018, doi:10.1029/2012JC007887.

1. Introduction

[2] The location of fronts in the Southern Ocean plays an important role in the global climate system. The latitude of the Subtropical Front (STF), for example, is thought to modulate the volume of warm and saline Agulhas Leakage in to the Atlantic, which in turn enhances the formation of North Atlantic Deep Water [*Bard and Rickaby*, 2009; *Beal et al.*, 2011; *Peeters et al.*, 2004]. However, the variability of both the strength and position of Southern Ocean fronts is still poorly understood. Ideally one would like to use direct observations to study the dynamics of fronts but in situ measurements from the Southern Ocean have historically been sparse and intermittent due to the remote location and harsh weather conditions. The available observations have been synthesized to produce valuable maps of the mean locations of Southern Ocean fronts [*Belkin and Gordon*, 1996; *Orsi et al.*, 1995] but the lack of repeat measurements means that little can be learned about the temporal variability.

[3] Satellite measurements now provide continuous high resolution observations of sea surface height (SSH) and sea surface temperature (SST), both of which can be used to identify ocean fronts [*Moore et al.*, 1999; *Sokolov and Rintoul*, 2002]. SSH measurements have been used to identify and track the movement of fronts across the Southern Ocean for periods of up to fifteen years [*Sokolov and Rintoul*, 2009]. This has revealed a great deal of information regarding the short-term temporal and spatial variability of fronts. For instance, correlations have been found between the location of fronts and the Southern Annular Mode (SAM) index [*Sallée et al.*, 2008]. Burls and Reason [2006] found that inter-annual and seasonal variability of subtropical SST frontal features in the central Atlantic Sector were related to changes in the wind stress field. However, this relationship does not hold close to the western boundary or the Sub-Antarctic Front (SAF). Large shifts in the position of fronts over topographic features have also been observed [*Sokolov and Rintoul*, 2009]. Nevertheless, at present the longest time series of satellite measurements available to analyze

[1]School of Environmental Sciences, University of East Anglia, Norwich, UK.
[2]Bert Bolin Centre for Climate Research, Stockholm, Sweden.
[3]Now at Department of Geological Sciences, Stockholm University, Stockholm, Sweden.
[4]Department of Geological Sciences, Stockholm University, Stockholm, Sweden.
[5]School of Mathematics, University of East Anglia, Norwich, UK.

Corresponding author: R. M. Graham, Department of Geological Sciences, Stockholm University, SE-106 91 Stockholm, Sweden. (robert.graham@geo.su.se)

0148-0227/12/2012JC007887

Southern Ocean fronts is approximately twenty years and thus provides limited information regarding the multidecadal variability of fronts or their response to climatic change.

[4] Paleo data can provide information on front positions in alternative climate states. For example, numerous studies suggest that ocean fronts were displaced northward during colder glacial intervals [*Bard and Rickaby*, 2009; *Howard and Prell*, 1992; *Kawagata*, 2001; *Nees et al.*, 1999]. However, the data used suffer from poor sampling resolution. Many studies use proxies for SST from a single core site [e.g., *Bard and Rickaby*, 2009; *Wells and Okada*, 1997]. This is insufficient to reconstruct temperature gradients and therefore conclusively locate fronts or identify frontal shifts [*Hayward et al.*, 2008; *Sikes et al.*, 2009]. A cooling signal similar to that caused by a frontal shift may be produced if there was a uniform cooling at the Last Glacial Maximum and no change to the SST gradient field [*Moore et al.*, 2000]. Care should therefore be taken when using paleo data to build our knowledge about the dynamics of Southern Ocean fronts and the response of fronts to changing climates.

[5] Theoretical arguments, based on Sverdrup dynamics, relate the location of Southern Ocean fronts and in particular the STF, to the overlying wind stress field [*De Ruijter*, 1982]. In line with this idea, climate change simulations using coarse resolution general circulation models show the Antarctic Circumpolar Current (ACC) to shift south in response to a warming climate and southward shift of the Southern Hemisphere westerly winds [*Fyfe and Saenko*, 2006]. This may be interpreted to suggest that fronts within the current would also shift south. However, the models used in these simulations are incapable of resolving frontal features or the complex topography of the Southern Ocean.

[6] Topography is known to play an important role in the dynamics of the Southern Ocean circulation [*Sinha and Richards*, 1999; *Tansley and Marshall*, 2001; *Thompson*, 2010]. Studies using quasi-geostrophic models have shown the structure and locations of jets are strongly influenced by the length scale of zonal ridges as well as the meridional slope of topography [*Thompson*, 2010]. Similar experiments indicate that the meridional spacing of jets is reduced when topographic slopes enhance the potential vorticity (PV) gradient [*Sinha and Richards*, 1999]. Observations also show that the ACC and Southern Ocean fronts are steered by the bottom topography [*Moore et al.*, 2000]. For example, the Campbell Plateau ($\sim$170° E) is a large topographic barrier to the ACC and flow is deflected south by several degrees of latitude around the feature [*Sokolov and Rintoul*, 2007]. The extent to which topography constrain fronts is still a topic of debate. Many studies assume that the latitude of fronts is constrained only close to steep topographic ridges, while they are free to move with changes to the wind field over regions of flat topography [*Hayward et al.*, 2008; *Howard and Prell*, 1992; *Kemp et al.*, 2010]. This has been supported by observations showing that fronts in these regions experience greater inter-annual variability compared with those close to steep topographic slopes [*Sallée et al.*, 2008; *Sokolov and Rintoul*, 2007, 2009]. However, it remains unclear whether this pattern will hold over decadal or longer timescales over which the Southern Hemisphere westerlies may experience a shift in position.

[7] Here we analyze 100 years of model output from a climate change simulation and a control simulation using the high resolution coupled climate model HiGEM [*Shaffrey et al.*, 2009]. The length of these simulations offers an opportunity to investigate multidecadal variability of Southern Ocean fronts. The climate change simulation was subject to a high level of increased CO_2 forcing that led to an intensification and 1.3° southward shift of the Southern Ocean winds. This small but significant shift allows us to study the response of fronts to a displacement in winds in a high resolution model.

[8] A description of the model is given in section 2, along with a discussion of how well different surface properties and methods perform at identifying jets and capturing their temporal variability. In section 3 comparisons are made between the mean location and structure of fronts in HiGEM and those from observations. The relationship between fronts and topography is then explored and we evaluate the response of fronts to the increased CO_2 forcing in the climate change simulation. A discussion is given in section 4, followed by a summary in section 5.

2. Methodology

2.1. Model Description

[9] The behavior of Southern Ocean fronts is analyzed in model output from HiGEM1.1. HiGEM is the UK's first high resolution global environment model and is built upon the UK Met Office's Unified Model HadGEM [*Roberts et al.*, 2009]. The model has a horizontal resolution of 0.83° latitude $\times$ 1.25° longitude in the atmosphere and 1/3° latitude $\times$ 1/3° longitude in the ocean. There are 38 vertical levels in the atmosphere and 40 in the ocean [*Shaffrey et al.*, 2009]. The oceanic resolution in HiGEM is eddy permitting and partially resolves these boundary currents and jets. Momentum dissipation occurs through a scale selective biharmonic scheme. Lateral mixing of tracers uses the isopycnal formulation of *Griffies* [1998] with constant isopycnal diffusivity. The *Gent and McWilliams* [1990] adiabatic mixing scheme with a latitudinally varying thickness diffusion and the adiabatic biharmonic scheme of *Roberts and Marshall* [1998] are used to parameterize eddies and reduce noise in tracer fields, particularly at high latitudes. To represent enhanced mixing at the ocean surface, temperature and salinity in the upper 20 m are mixed horizontally using a biharmonic scheme. The improved representation of steep horizontal gradients in temperature and velocity across Southern Ocean fronts in HiGEM, compared with coarser resolution models such as HadGEM [*Shaffrey et al.*, 2009], makes HiGEM ideal for the purpose of this study. For a complete model description see *Roberts et al.* [2009] and *Shaffrey et al.* [2009].

[10] The climate change and control simulations analyzed here are each 100 model years in length. Both simulations were initiated from a 30 year model spin-up under control simulation boundary conditions. CO_2 concentrations were fixed at 345 ppm in the control simulation. In the climate change simulation CO_2 concentrations increased by 2% per year for 70 years until concentrations reach four times that in the control simulation and were then kept constant for a further 30 years. For further information regarding the

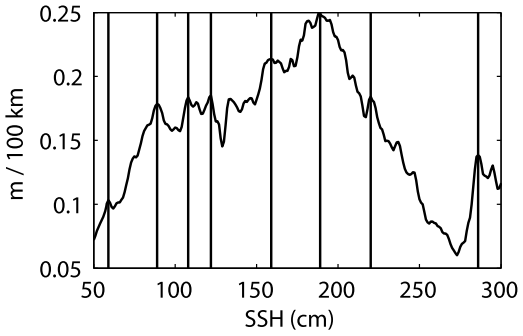

Figure 1. Mean zonal average SSH gradient in SSH space for a 4 year period in the control simulation. Vertical black lines show the SSH values for our SSH contour defined fronts.

climatological forcings in the control simulation see *Shaffrey et al.* [2009].

[11] The inter-annual variability of the fronts is investigated using annually averaged output. For the comparison of the climate change and the control experiments, the mean states of the last 30 years of each simulation are used. During this time period the CO_2 concentration was constant in both runs. Using the mean fields of the final ten years of each simulation gives similar results to those discussed in this paper. The high resolution of this model makes it computationally demanding, and it is therefore not feasible to run the model to equilibrium. However, by comparing the mean states between the same period of the climate change and control simulations the effects of model drift should be minimized.

2.2. Method of Identifying Fronts

[12] The criteria used to identify fronts vary widely between different studies and this has resulted in some confusion within the literature [*Sokolov and Rintoul*, 2007]. The criteria used are often dependent upon what data are available. Studies using hydrographic measurements often define fronts using subsurface properties [*Belkin and Gordon*, 1996; *Orsi et al.*, 1995] while more recent studies use surface signatures, such as SSH and SST gradients, to take advantage of the continuous high resolution data sets from satellites [*Billany et al.*, 2010; *Burls and Reason*, 2006; *Kostianoy*, 2004; *Moore et al.*, 1999; *Sokolov and Rintoul*, 2002]. In a model one can use any of the above methods and it therefore provides a useful test bed for comparing the effectiveness of different properties and methods for identifying fronts.

[13] Many recent studies follow the method of *Sokolov and Rintoul* [2007] to assign a specific SSH contour to each frontal branch and define this contour as the front's circumpolar path [*Billany et al.*, 2010; *Sallée et al.*, 2008; *Sokolov and Rintoul*, 2009]. To examine the performance of this method for monitoring short-term frontal variability in HiGEM, we analyze monthly output from a random four year period of the control simulation. Following the method of *Volkov and Zlotnicki* [2012], we calculate the time mean SSH gradients over the Southern Ocean for this 4 year period and zonally average the gradients along lines of constant SSH (rather than along latitude lines) (Figure 1). The SSH values that have a local maximum in SSH gradient are assumed to correspond to a particular front. The time mean location of these contours overlay regions of increased SSH gradient which indicates that the method performs well at identifying the mean location of fronts (not shown). However, the method performs less well at monitoring the temporal variability of fronts. For example, at 240°E it is clear from the SSH gradient field that there is a front present at ~62°S for the whole duration of the time interval (Figure 2b). One of our selected contours tracks the position of this front well for the first ~30 months but then shifts south and begins meandering over a 3° range. Similarly, at 265°E our SSH contours correspond well to the position of fronts visible in the SSH gradient field, between 55°–70°S, throughout most of the interval (Figure 2c). However, there is a ~3 month period after 43 months where the contours are

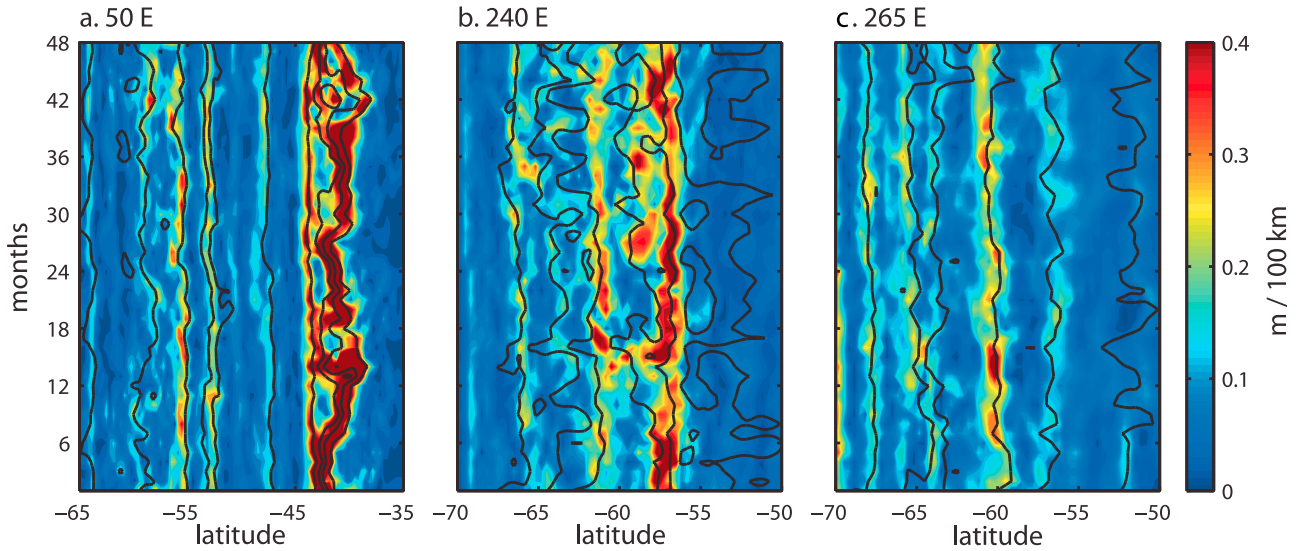

Figure 2. Time series of SSH gradient over a 4 year period in the control simulation at 3 longitudes. (a) 50°E. (b) 240°E. (c) 265°E. Black contours correspond to the SSH values given in Figure 1.

Table 1. The Performance of Three Alternative Variables for Identifying Fronts

Method of Identifying Front (Local Maxima in)	Threshold Value	Color
Zonal Transport	10 Sv / 100 km	Black
SSH Gradient	0.1 m / 100 km	Cyan
SST Gradient	-	Magenta
	0.8 K / 100 km	Yellow

displaced north while the location of fronts remains constant. Nevertheless, these discrepancies are intermittent and localized. For example, at 50°E the method performs very well (Figure 2a).

[14] The key limiting factor of the SSH contour approximation method is that SSH gradients are not enhanced at all points along each contour around the circumpolar belt [*Sokolov and Rintoul*, 2002]. Thus movement of a contour associated with a front does not always imply that a front has shifted. For example, at 240°E the northernmost contour visible in the domain is not associated with a front at this longitude. Here the contour is meandering over a range in excess of 5 degrees (Figure 2b). Similarly at 265°E the northernmost SSH contour meanders between 50°S–54°S, while no front is visible in the SSH gradient field. A front is only present during the first 6 months of the 4 year period here, during which time the front and contour have a constant latitude (Figure 2c). The meridional displacements of these SSH contours, where no front is present, do not reflect variability in the location of a front. However, the variability of the contours would be included in zonal or basin average positions of the fronts, calculated using these contours, and therefore suggest spurious frontal movement. The SSH contour method is still an invaluable tool, but frontal shifts must be confirmed by a change in the SSH gradient field [*Sokolov and Rintoul*, 2009].

[15] We next compare the performance of three alternative variables for identifying fronts namely; SST gradients, SSH gradients, and zonal transport (Table 1). The meridional and

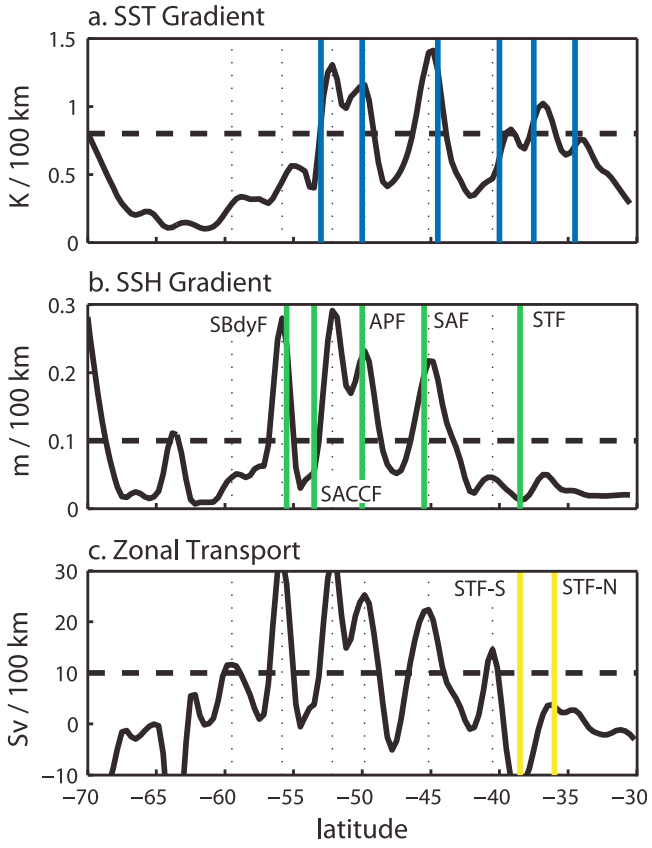

Figure 3. Front locations from observations (color) and a comparison of methods for identifying fronts along a transect at the Greenwich Meridian (0°E): (a) magnitude of SST gradient, (b) magnitude of SSH gradient, and (c) zonal transport (surface to bottom). Properties are averaged over the final 30 years of the HiGEM control simulation. The threshold values used to identify fronts in Figure 4 are indicated by horizontal dashed lines. The vertical black dotted lines show the location of fronts identified using our zonal transport method (see Table 1). Observation data is as follows: in Figure 3a, blue lines are local maxima in the SST gradient field for July (2002–2004) exceeding our threshold of 0.8 K / 100 km [*Burls and Reason*, 2006, Figure 3], in Figure 3b, green lines are positions of fronts identified using SSH gradient data from 1993 and 2007 [*Billany et al.*, 2010], and in Figure 3c, yellow lines are northern and southern branches of the STF identified using surface geostrophic velocities calculated from SSH data between 1992 and 2007 [*Dencausse et al.*, 2011]. The observed fronts are labeled where names are given in the relevant study.

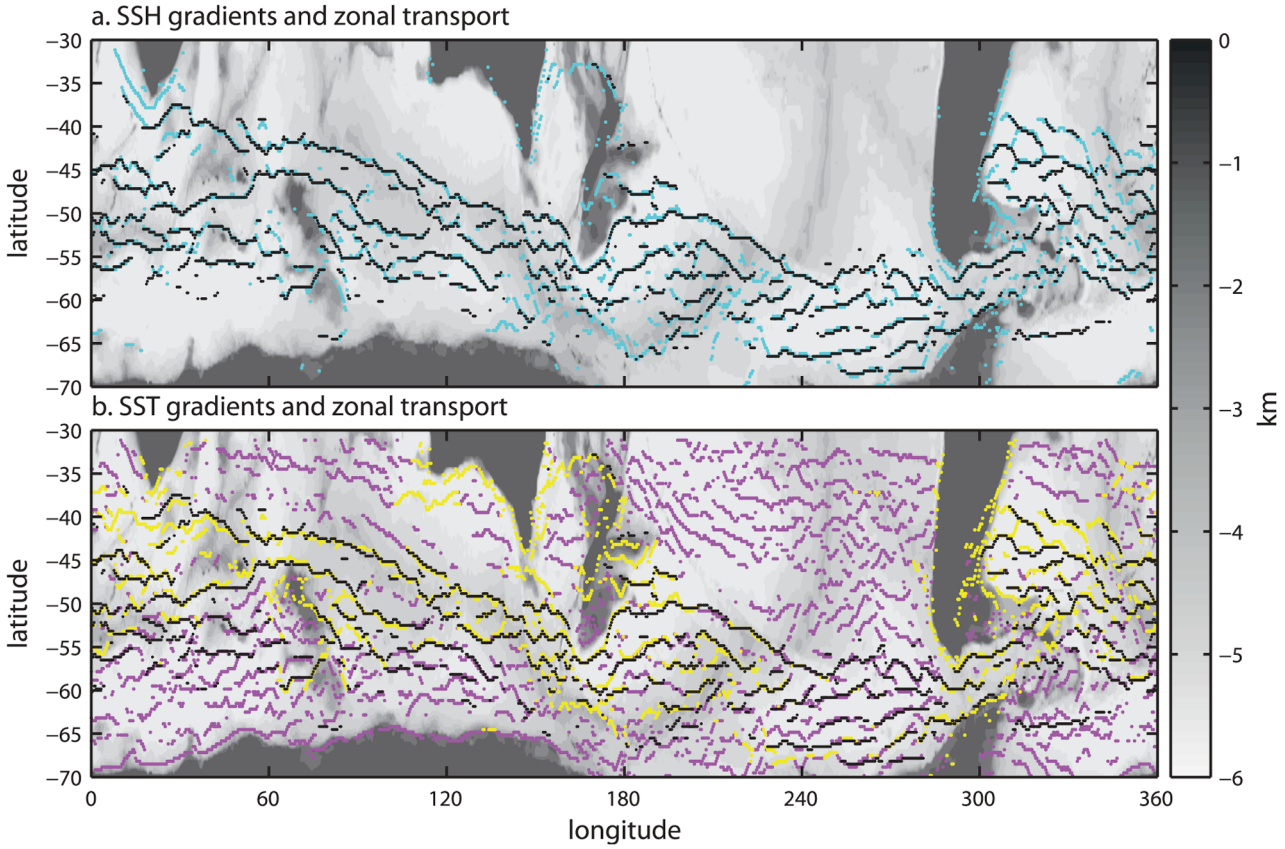

Figure 4. The mean location of Southern Ocean fronts for the final thirty years of the control simulation in relation to the model topography. (a) SSH fronts (cyan) and zonal transport fronts / jets (black). (b) SST fronts (yellow) and jets (black). Magenta dots indicate the locations of local maxima in the SST gradient field where the magnitude does not exceed the threshold value shown in Figure 3.

zonal SSH and SST gradients are calculated across each grid point using neighboring points (centered difference) for individual years. The magnitude of the resultant gradient vector is then calculated at each point. Units are given in m/100 km and °C/100 km for SSH and SST gradients respectively. The zonal transport is calculated by vertically integrating the total zonal velocity from the ocean surface to the ocean floor and multiplying it by the meridional extent of the grid box. Units are then converted from $m^3/s/0.33°$ latitude to 10^6 $m^3/s/100$ km (i.e., Sv/100 km). The analysis was repeated using a shallower uniform depth for the integration and this was found to have little impact on the results. For each of these three variables, fronts are identified as all the local maxima across a meridional transect (30°S–70°S) of each property that exceed a threshold value (Table 1 and Figure 3). The threshold values are chosen so that the number of fronts identified is roughly consistent with *Sokolov and Rintoul* [2007]. These values are somewhat arbitrary but altering them was found to have no effect on the main conclusions drawn from this study.

[16] The locations of SSH fronts coincide with jets (zonal transport fronts) in almost all cases (Figure 4a), as should be the case in a flat-bottomed geostrophic ocean, and there is a near-linear relationship between the magnitudes of the two properties (Figures 3b and 3c). Thus jets associated with the ACC fronts can be easily identified in the SSH gradient field, and the magnitude of the gradient can be used as a suitable proxy for the intensity of the jet. In contrast, local maxima in SST gradient are not always coincident with the core of a jet (e.g., 40.5°S, Figure 5). Where deep isotherms tilt toward the surface the maximum in SST gradient is located south of the transport and SSH gradient maximum. Nevertheless, fronts can still be identified and tracked by the SST gradient signature. SST gradient maxima coincide more closely with the core of jets in fronts located further south (Figure 5).

[17] Surface temperature and salinity gradients across the STF are density compensating in some regions [*Sokolov and Rintoul*, 2002] and as a result there is no SSH gradient or transport associated with the front at these locations (e.g., 37°S, Figure 3). This provides strong motivation for using the SST gradient to identify the STF rather than SSH gradient or zonal transport. Interestingly our SST gradient method does not identify a clear continuous STF around the circumpolar belt, as was described by *Orsi et al.* [1995] and *Belkin and Gordon* [1996] (Figure 4b). However, these studies were based on limited hydrographic data available at that time. The question of whether a continuous STF exists between the Atlantic and Indian sectors of the Southern Ocean has been the focus of a number of more recent dedicated studies and remains a topic of debate [*James et al.* 2002; *Burls and Reason*, 2006; *Dencausse et al.*, 2011].

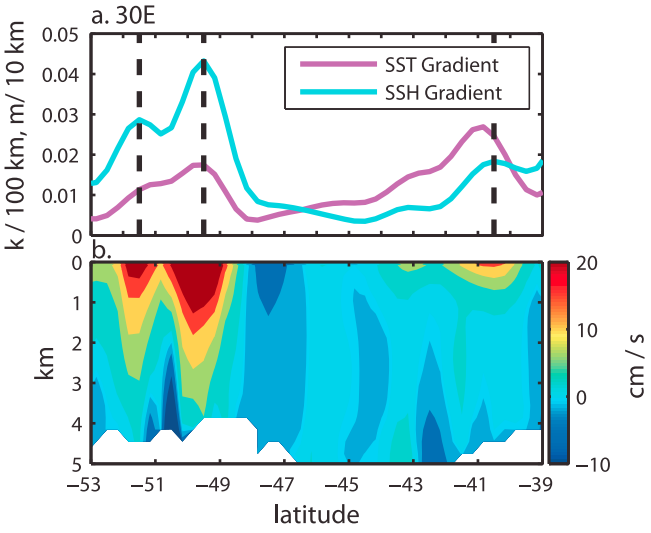

Figure 5. Meridional transect at 30°E. Values are 30 year means for the control simulation. (a) SSH (cyan) and SST (magenta) gradient. Vertical black dashed lines show the location of fronts identified using our zonal transport method. (b) Zonal velocity.

Here the fronts identified using the SST gradient method (yellow dots, Figure 4b) are consistent with observations of the STF based on recent satellite data. For example, in the Atlantic Sector *Burls and Reason* [2006] identified a SST front close to the western boundary at 40°S. This front then meandered southeast to join the SAF. In the central Atlantic (10°W–10°E) various front-like features were identified between 35°S–40°S that dissipated to the west. Further east these fronts were found to merge with the Agulhas current. These patterns are replicated in the output from HiGEM (Figure 4b). The locations of high SST gradients associated with the STF in HiGEM are also broadly consistent with observations from the Indian Sector [*Kostianoy*, 2004; *James et al.*, 2002].

[18] Large scale variations in the background SST gradient over the Southern Ocean preclude a consistent definition of a front that can apply everywhere [*Kostianoy*, 2004]. Background SST gradients are weaker in the cold waters further south. Therefore SST gradients across fronts at southern latitudes are relatively weak, despite the often large transport, in comparison with frontal features in the north (56°S, Figure 3). Hence, the SST gradient is a poor proxy for the intensity of a jet. This is particularly apparent in the eastern Pacific Sector where all fronts are at their southernmost extent before entering Drake Passage (Figure 4b). To identify these frontal features from the SST gradient field a low threshold must be used. However, this introduces considerable noise more equatorward by identifying spurious fronts in regions of the ocean where background SST gradients are higher (Figure 4b). Thus while the SST gradient method performs better at identifying the STF, the SSH gradient method is more successful at identifying jets located further south and is therefore a more suitable tool for studying fronts over the entire Southern Ocean. SST gradients become a more useful tool if one can reduce the size of the study area and thereby the variations in the background SST gradient. This makes it is easier to distinguish local maxima in SST gradients from the background [*Kostianoy*, 2004].

[19] Here, we study fronts over the entire Southern Ocean and are most interested in those that are associated with jets. Therefore we use the zonal transport method to identify fronts throughout the rest of this study. Fronts will be identified by local maxima in the zonal transport field, where the zonal transport exceeds a threshold value of 10 Sv / 100 km (Table 1).

3. Results: Southern Ocean Fronts in HiGEM

3.1. Validation Against Observations

[20] To validate the performance of the model in reproducing reasonable frontal structure, we first compare the latitude of fronts in HiGEM with observations at the Greenwich Meridian, 0°E (Figure 3) [*Billany et al.*, 2010; *Burls and Reason*, 2006; *Dencausse et al.*, 2011]. Figure 3 indicates the location of fronts identified in these studies, each using different properties, for comparison with the time-mean SSH and SST gradient fields and zonal transport from the HiGEM control. Overall HiGEM captures the positions of the primary ACC fronts (SAF and Antarctic Polar Front (APF)) well at this longitude. Our zonal transport method locates a front with mean latitude of ∼45°S at the Greenwich Meridian in HiGEM. This sits between the estimated location of the SAF from both *Billany et al.* [2010] and *Burls and Reason* [2006] (Figures 3a and 3b). Similarly, there is a front at 50°S in HiGEM that corresponds exactly to the position of the APF given by these two previous studies. A difference between the observations and the model is that the front at 50°S, in HiGEM, has a southern branch located at 52°S. We define this feature as a branch due to the fact the minimum transport (and gradients) between the two local maxima is above our threshold criteria (Figure 3). In contrast there was a clear minimum in SSH and SST gradient between the APF and the fronts located at 53.5°S and 53°S, found by *Billany et al.* [2010] and *Burls and Reason* [2006] respectively. *Billany et al.* [2010] label the front at 53.5°S as the Southern ACC Front. In HiGEM the Southern ACC Front may have merged with the Southern Boundary Front, located at 56°S, at this longitude. We suggest this because the magnitude of the SSH gradient across this front in HiGEM is more than double that observed by *Billany et al.* [2010].

[21] It is difficult to assess the vertical structure of the fronts accurately due to limited available observations at depth. However, repeat observations have been made along the WOCE SR3 transect at ∼140°E [*Rintoul and Sokolov*, 2001; *Sokolov and Rintoul*, 2002]. In Figure 6b we show a cross section of the mean neutral density anomaly in the control simulation at this longitude. This compares well to the observations in these papers. Fronts can be identified by the lifting of isopycnal surfaces in these plots. In Figures 2 and 11 of *Sokolov and Rintoul* [2002] and Figure 2 of *Rintoul and Sokolov* [2001], two fronts can clearly be seen in the neutral density anomaly, extending from the ocean surface to the ocean floor, at ∼62°S and ∼64°S. These same features are visible here in Figure 6b. We also plot the mean zonal velocity so that these jets can easily be identified (Figure 6a). The cross section at 30°E (Figure 5) corresponds to a section studied by *Sparrow et al.* [1996], using

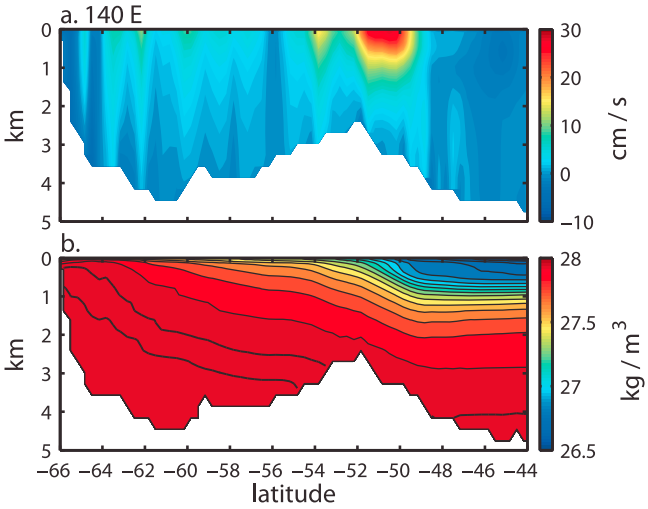

Figure 6. Meridional transect at 140°E. Values are 30 year means for the control simulation. (a) Zonal velocity. (b) Neutral density anomaly.

the HASO data set and the Fine Resolution Antarctic Model (FRAM). The zonal velocity fields from HiGEM and FRAM are consistent with the HASO data. All 3 show a shallow STF located at ~40°S, where the transport is confined to the upper layers, and a stronger more barotropic front at ~50°S, which *Sparrow et al.* [1996] label the APF.

[22] We see that the position and structure of fronts in HiGEM correspond well to past observational studies at these three longitudes (0°E, 30°E and 140°E). Nevertheless, fronts are highly variable around the circumpolar belt. In Figure 7 we compare the locations of fronts identified by *Sokolov and Rintoul* [2009] with the mean zonal transport field in the HiGEM control simulation. There are discrepancies, but in most cases the strong jets in HiGEM are in close proximity to one of the fronts identified by *Sokolov and Rintoul* [2009]. These comparisons with observations provide some confidence that HiGEM is capturing the dynamical processes important to fronts and should therefore respond to the climate change forcing in a similar manner to the real ocean.

3.2. Fronts and Topography

[23] The number of fronts in HiGEM varies strongly with longitude (Figure 8b). There are less fronts in regions where the flow is restricted by topography, such as at the Kerguelen Plateau (70°E), the Campbell Plateau (170°E), and Drake Passage (300°E). The peak intensity of the strongest front at each longitude, which we define as the maximum zonal transport at any latitude between 30°S and 70°S, increases by a factor of two or more in these regions (Figure 8a). Downstream of these topographic obstacles the number of fronts increases as the channel widens and the intensity of fronts weakens. *Thompson et al.* [2010] also studied the relationship between number of fronts and topography using two years of output from an eddy-resolving ocean general circulation model. The mean number of fronts was inferred by the number of distinct homogenized potential vorticity (PV) pools on each density surface. Similar patterns were found to those presented here despite the different models and methods used to identify fronts. Here we also see visible inter-annual variability in the number of fronts. The number of fronts identified at each longitude is not constant. However, there are no large scale trends in the number of fronts as a result of the climate change forcing. While locally there are significant decreases in the peak intensity of fronts at some longitudes (e.g.145°E, Figure 8a), the large scale zonal pattern (of peak front intensity increasing in the vicinity of major topographic features) remains constant between the control and climate change simulation. These findings indicate that zonal variations in the number and intensity of fronts are strongly controlled by the bottom topography.

[24] We examine how local topography influences jet location in HiGEM by plotting meridional cross sections of zonal velocity, averaged over the final 30 years of each simulation, at ten-degree intervals (e.g., Figures 5b and 6a). No consistent patterns of where jets are positioned in relation to the underlying topographic gradients were identified

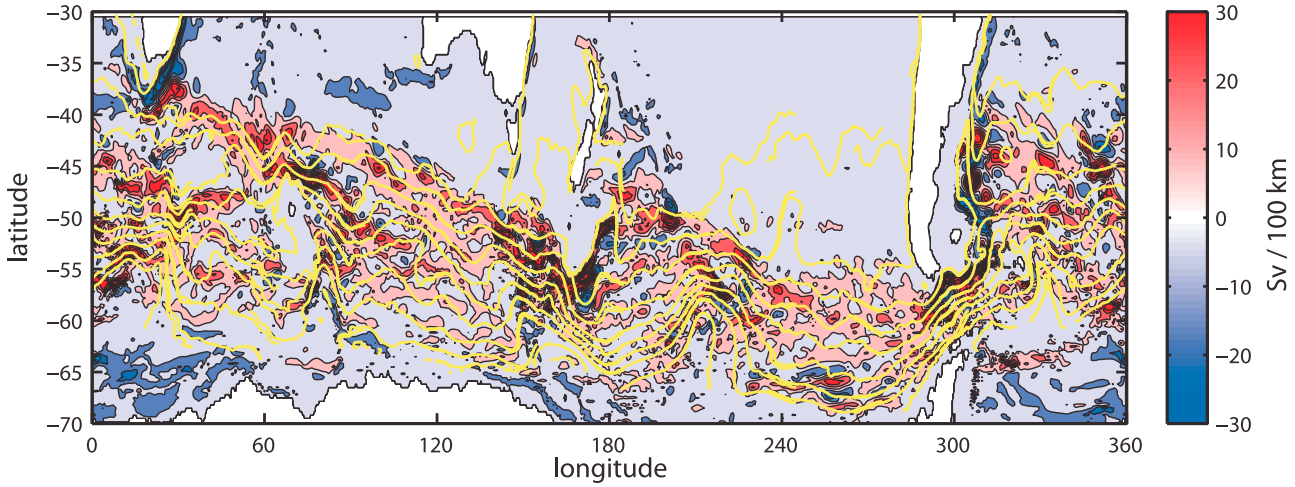

Figure 7. Mean zonal transport field (surface to bottom) for the final 30 years of the control simulation and location of fronts given by *Sokolov and Rintoul* [2009] (yellow). The northernmost front shown is defined as the Southern Subtropical Front.

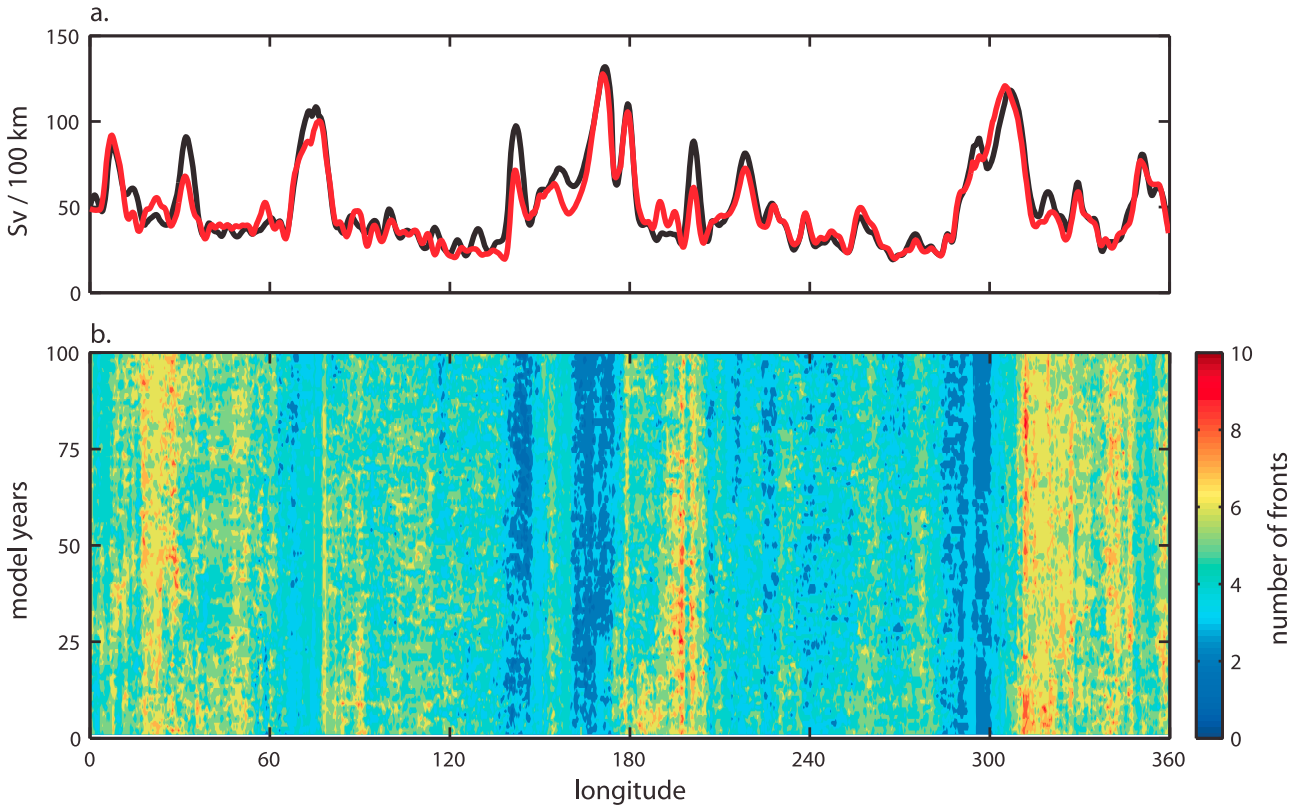

Figure 8. (a) Maximum zonal transport between 30°S and 70°S at each longitude, averaged over the final 30 years of both the control (black) and climate change (red) simulations. (b) Number of fronts as a function of longitude and time for the climate change simulation.

from the cross sections studied. We did not observe steady jets fixed to the strongest topographic gradients or unsteady jets meandering from regions of enhanced to reduced PV gradients, as may be expected from the findings of *Thompson* [2010]. At some locations the jets do lie over strong topographic gradients (e.g., 51°S, Figure 6a) but elsewhere jets are found over flat bottom sections (e.g., 52°S, Figure 5b). In contrast to findings from quasi-geostrophic models, we do not find a consistent relationship between the meridional topographic gradient and the spacing between jets [*Sinha and Richards*, 1999]. This relationship also broke down in a shorter high resolution simulation on the Parallel Ocean Program (POP) general circulation model [*Sinha and Richards*, 1999]. It is likely that this is due to the complex bottom topography in the Southern Ocean of both HiGEM and POP. In contrast the quasi-geostrophic models used by *Sinha and Richards* [1999] and *Thompson* [2010] included only zonal ridges or sinusoidal bumps. *Tansley and Marshall* [2001] show that up and downstream topographic features can have strong influences on jets and this may explain why studying the meridional transects individually here does not lead to any strong conclusions. The complex topography of the Southern Ocean makes it difficult to attribute the effect of individual topographic features to fronts. In order to improve our understanding of how bottom topography influences the dynamics of fronts, further idealized modeling studies are required, following the work of *Sinha and Richards* [1999], *Tansley and Marshall* [2001] and *Thompson* [2010].

3.3. The Response of Fronts to a Southward Shift in Winds

[25] As a result of the increased CO_2 concentrations in the HiGEM climate change simulation, the Southern Hemisphere midlatitude westerly winds intensify and shift south (Figure 9a and 10b). Specifically, the maximum zonally averaged zonal wind stress strengthens by 13% from 0.176 Nm^{-2} to 0.199 Nm^{-2} and shifts south by 1.3° latitude from 51.5°S to 52.8°S (Figure 10b). An intensification and southward shift of the westerlies in response to increased CO_2 forcing is a robust result in many climate change modeling experiments [*Fyfe and Saenko*, 2006; *Kushner et al.*, 2001; *Saenko et al.*, 2005; *Sen Gupta et al.*, 2009; *Spence et al.*, 2010].

3.3.1. Changes Within the ACC

[26] The path of the ACC, defined here as the flow between the northernmost and southernmost streamlines passing through Drake Passage, contracts in the climate change simulation (Figure 9c). There is a small southward shift of the current's southern limit between 120°E and 160°E but at all other longitudes the southern boundary moves north or remains fixed. Similarly, the northern limit of the current moves south or remains fixed at all longitudes. Therefore, in contrast to results from coarser resolution models that suggest the ACC moves south in response to a southward of the winds [*Fyfe and Saenko*, 2006; *Saenko et al.*, 2005], we find no net meridional displacement of the current's path. This may either be because the wind shift

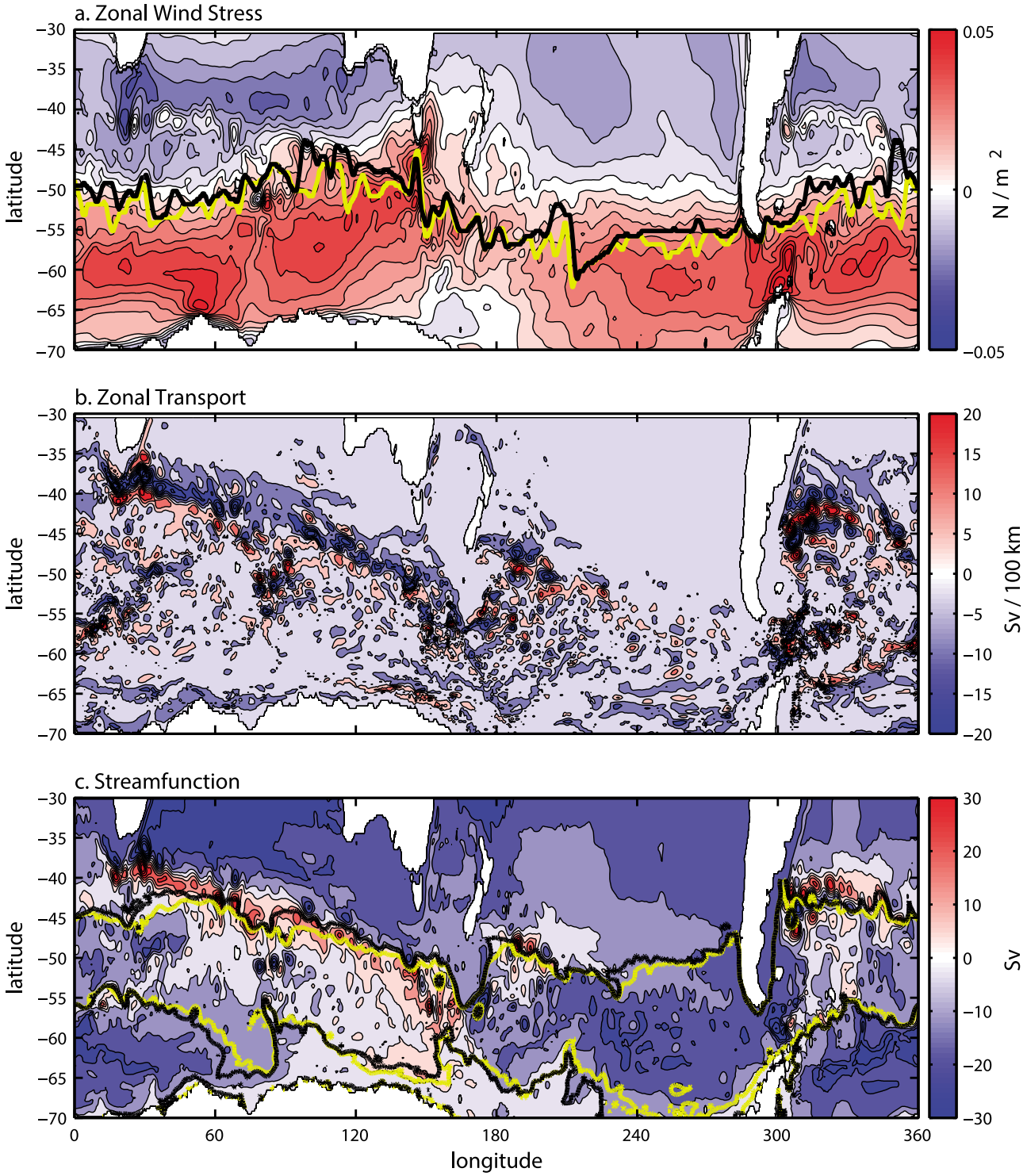

Figure 9. (a) Mean zonal wind stress anomaly. The location of the maximum wind stress for the control (black) and climate change (yellow) is also shown. (b) Mean zonal transport (surface to bottom) anomaly. (c) Mean barotropic stream function anomaly. The location of the northernmost and southernmost streamlines passing through Drake Passage for the control (black) and climate change (yellow) is also shown.

is not large enough, or because the coarse resolution models do not resolve the fronts and topography within the ACC adequately.

[27] The volume transport through Drake Passage, calculated by meridionally integrating the full depth zonal transport, decreases from an average value of 176 Sv in the control simulation to 162 Sv in the climate change simulation despite the increased wind stress over the Southern Ocean. A reduction in ACC transport in response to strengthening winds over the Southern Ocean has been

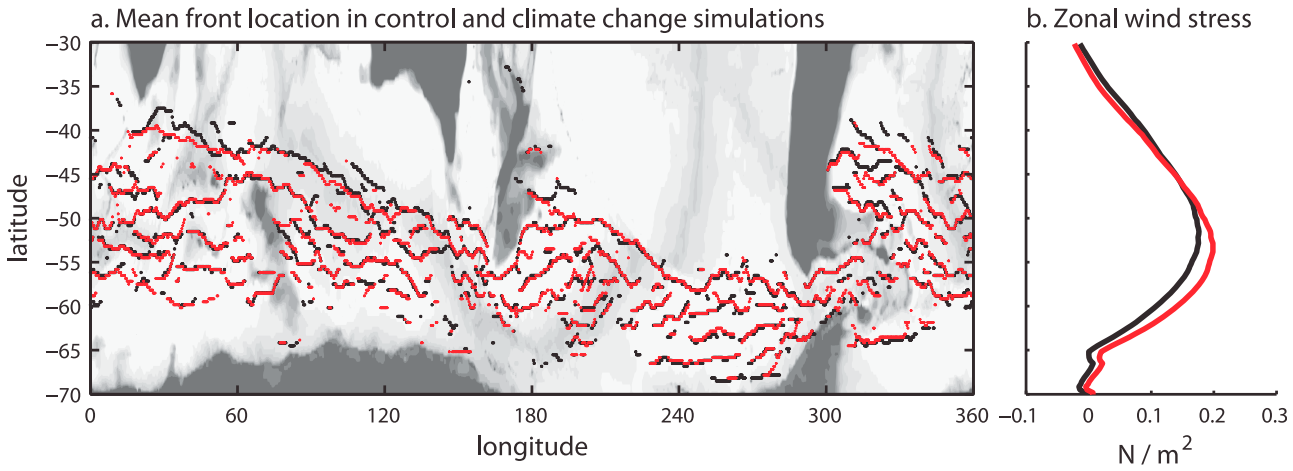

Figure 10. (a) Mean location of fronts for the final 30 years of the control (black) and climate change (red) simulations (model topography shown in gray scale). (b) Mean zonal average zonal wind stress for the final 30 years of the control (black) and climate change (red) simulations.

found in a number of recent studies using higher resolution models [*Hogg*, 2010; *Wang et al.*, 2011]. *Hogg* [2010] suggests that the increased wind stress enhances eddy mixing and therefore reduces the meridional density gradients which enhance the flow. Similarly, *Wang et al.* [2011] propose that the decrease in transport results from a combination of expanding subtropical and subpolar gyres, which reduces the width of the ACC, and enhanced eddy mixing which prevents isopycnal surfaces from steepening. Thus a narrower ACC results in less transport. In HiGEM the width of the ACC is also reduced in the climate change simulation (Figure 9c) and there is indication that the suptropical gyres expand. The location of the maximum SSH in the center of the South Atlantic subtropical gyre shifts southwards by 3° latitude in the HiGEM climate change simulation and the location of the maximum in the Indian Ocean shifts south by 2° (not shown). The zonal transport and barotropic stream function anomalies also suggest an intensification of the Weddell Gyre (Figures 9b and 9c).

[28] The mean locations of fronts were mapped for the final thirty years of both the climate change and control simulation (Figure 10a). The most significant changes between the two simulations in the location of fronts (Figure 10a) and circulation (Figure 9b) take place north of the circumpolar transport (discussed in section 3.3.2). The movement of most fronts within the boundaries of the ACC is minimal compared with the 1.3° average southward shift in winds. A localized region within the ACC where we do see a shift of fronts is in the lee of the Kerguelen Plateau (80°E, Figures 9b and 10a). Interestingly there is little change in the latitude of the maximum wind stress over this region (Figures 9a and 11b). At 80°E there is a relatively abrupt ∼1.5° northward shift of the front located at ∼52.5°S around thirty years into the simulation (Figures 11e and 11h). While this front has shifted north at 80°E, it can be seen that there is still a weak local SSH gradient maximum at its previous mean latitude (Figure 11e). The front at ∼42.5°S, associated with the Agulhas return current, has also weakened at this longitude (Figures 11e and 11h) but there is little change in the mean intensity or latitude of any other fronts.

[29] A 25% increase in the maximum wind stress is observed over fronts in the Pacific Sector in the climate change simulation compared with the control, and there is a ∼2° southward shift of the latitude of maximum wind stress between 240°E–270°E (Figure 9a). This is a region of relatively flat bathymetry where topography should have little constraint on fronts [*Hayward et al.*, 2008; *Sallée et al.*, 2008]. However, this major change in wind-forcing appears to have little effect on the location of fronts (Figure 10a). For example, the maximum zonal wind stress at 265°E increases by 17% in the climate change simulation (Figure 11c). In fact, over the most intense front at 60°S, the southward shift of the wind field results in as much as 28% increase in wind stress. While there is a slight indication of the more northern jets intensifying and southern jets weakening at this longitude, there is no discernible difference in the locations of frontal jets (Figures 11f and 11i).

[30] The mean zonal transport anomaly shows signs of a northward shift, which may be associated with movement of fronts, centered around 255°E (Figure 9b). Here the location of the maximum wind stress has shifted south by ∼3° (Figure 9a and 12a), and so one may expect a shift of fronts at this location. The mean transport fields of the climate change and control simulation at this longitude show a weakening of the southernmost jet and indicate that the jet located at ∼63°S has intensified and shifted north by ∼0.5°, but no other jets show sign of movement (Figure 12b). Meanwhile Hovmöller diagrams of SSH gradients for the control and climate change simulation at this longitude show that the jet at 63°S has large inter-annual variability in intensity and is not tightly constrained to a narrow latitude band (Figure 12c and 12d). No clear shift of fronts is visible from the time series of SSH gradients alone, and so the shift of transport does not appear to be significant in relation to the inter-annual variability here. Thus there is little evidence to suggest any large scale shifts of fronts in the Pacific Sector as a result of the climate change forcing. In particular, the movement of fronts is not of a comparable magnitude to the zonal average 1.3° southward shift of the maximum wind

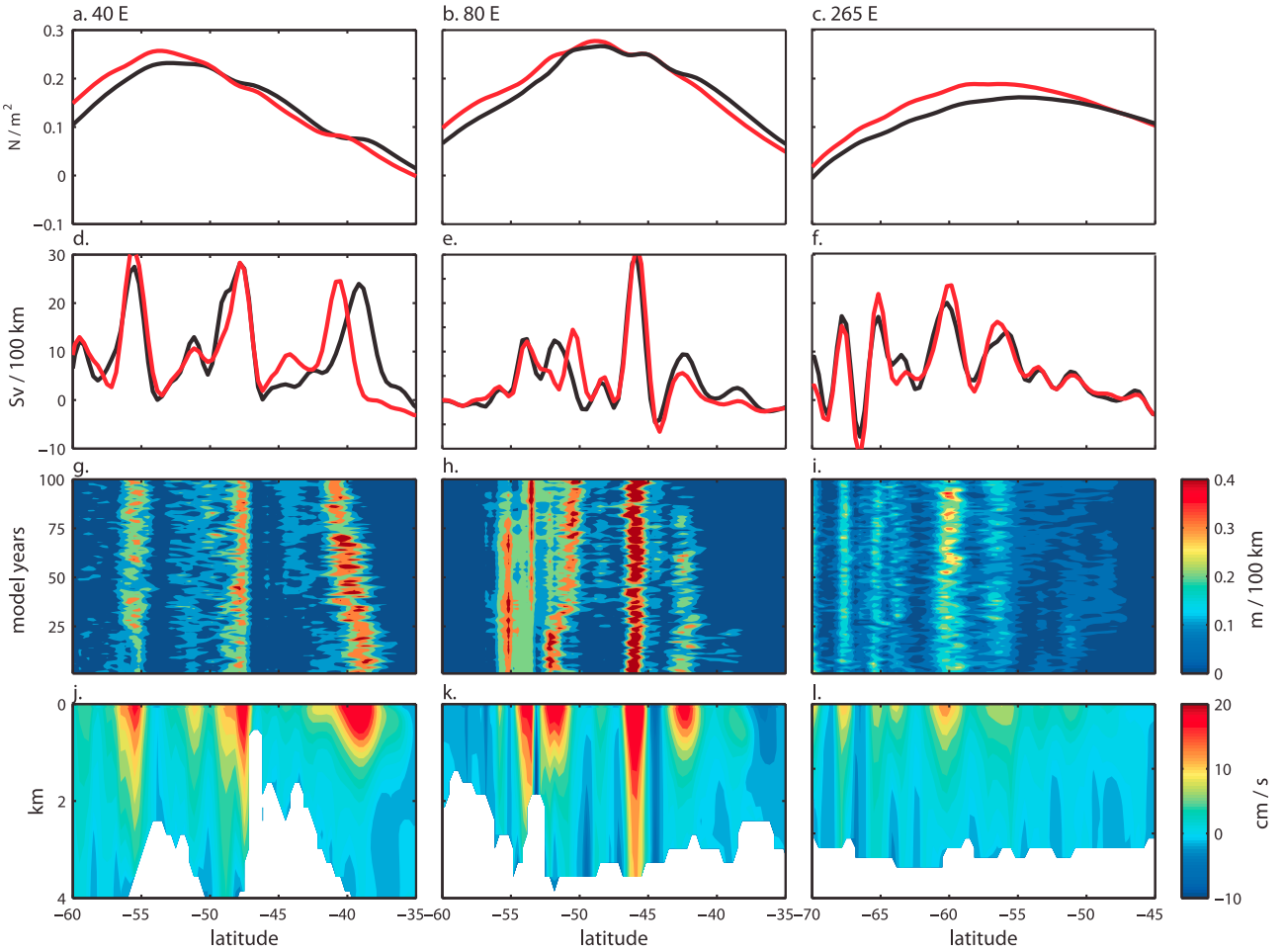

Figure 11. Meridional transects along (left) 40°E, (middle) 80°E and (right) 265°E. Line plots show (a–c) mean zonal wind stress and (d–f) mean zonal transport for the final 30 years of the control (black) and climate change (red) simulations. The *y* axis in Figure 11e ranges from −20–60 Sv/100 km. (g–i) Hovmöller diagrams of SSH gradient magnitude in the 100 year climate change simulation. (j–l) Mean zonal velocity for the final 30 years of the control simulation. The color scale saturates at 20 cm/s and the *y* axis in Figure 11l ranges from 0–6 km.

stress. A similar pattern is found for most fronts within the ACC boundaries (Figure 10a).

[31] Some studies suggest the extent of Antarctic sea-ice can influence the location of, or can be used as a proxy for, the APF [*Moore et al.*, 2000; *Nürnberg and Groeneveld*, 2006]. The sea-ice in HiGEM retreats southwards during the climate change simulation (not shown) by more than 5° latitude at some longitudes (e.g., 100°E). However, there is little meridional movement of fronts in these regions (Figure 10a). Moreover, the contraction of the circumpolar transport and the zonal transport anomalies (Figures 9a and 9c) suggest that any movement of southern fronts are northward, consistent with the theory of expanding subpolar gyres [*Wang et al.*, 2011] and enhanced northward Ekman transport [*Sallée et al.*, 2008]. Thus there is no evidence in our results to suggest that changes to Antarctic sea-ice can influence the location of any ACC fronts.

3.3.2. Changes to the STF and Agulhas Front

[32] Major changes to the intensity and position of Southern Ocean fronts in the climate change simulation are confined to western parts of the Atlantic and Indian sector, north of the circumpolar transport (Figures 9b and 10a). These fronts which shift correspond closely to the location of the Southern STF [*Sokolov and Rintoul*, 2009] (Figure 7) and Agulhas Front [*Belkin and Gordon*, 1996]. In the Indian Sector the Southern STF front lies several degrees south of the more density compensated Northern STF. At 120°E roughly 10 degrees latitude separates these features in HiGEM. Here the Northern STF is located at 37°S and can be detected only by our SST gradient methods (Figure 4b, yellow lines) as there is no strong jet or SSH gradient associated with it (Figure 4a). In contrast the Southern STF which is located at 47°S can be detected by all three of our methods (Figure 4). The Southern STF in the Indian sector lies just north of the ACC boundary (Figure 9c) and shifts south by up to 3 degrees latitude as a result of the climate change forcing (e.g., 30°E, Figure 10a). There is a large-scale southward shift of transport associated with the movement of the STF here (Figure 9b). This shift happens gradually and in some places occurs over steep topographic

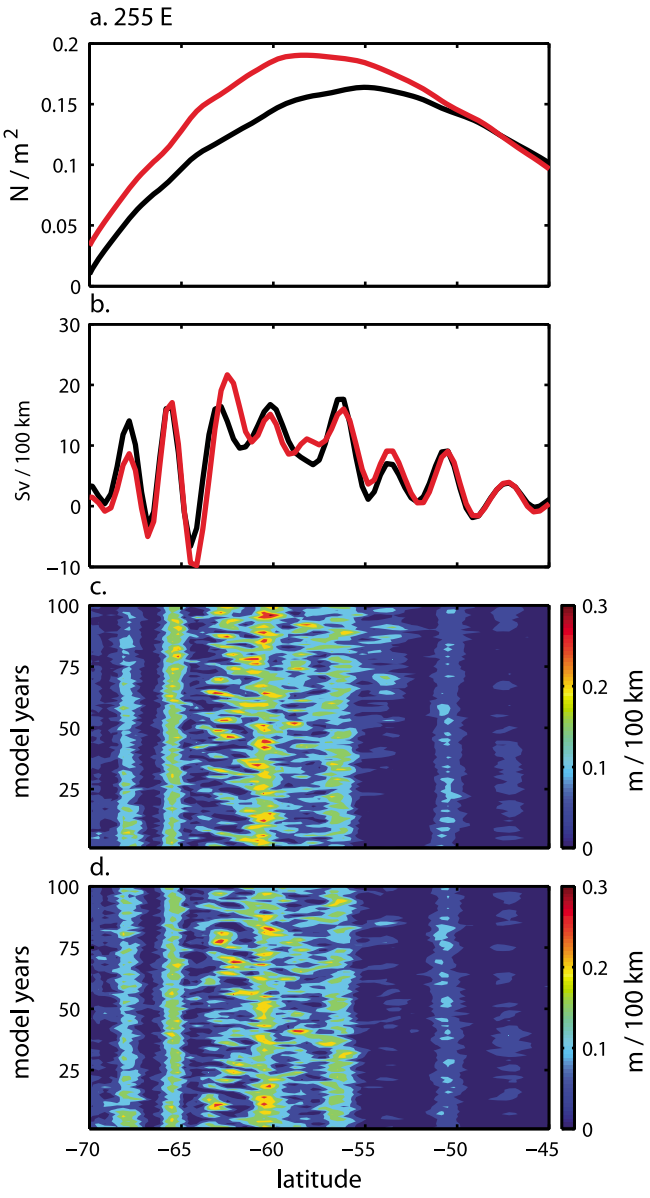

Figure 12. Meridional transects along 255°E. Line plots show mean values for the final 30 years of the control (black) and climate change simulations (red). (a) Mean zonal wind stress. (b) Mean zonal transport. (c) Hovmöller diagram of SSH gradient magnitude in the 100 year climate change simulation. (d) Same as Figure 12c but for control simulation.

ridges (e.g., 40°E, Figures 11d and 11j). It is interesting that the movement of fronts is confined to the Atlantic and Indian Sectors of the Southern Ocean (Figures 9b and 10a). East of the Campbell plateau, at 200°E, the southward shift ceases.

[33] As the Agulhas Front and STF shift southwards over the Indian Sector the intensity of the fronts decreases. This can be seen from the mean zonal transport anomaly (Figure 9b). This weakening may in part be the result of a reduction in the Indonesian Throughflow, one of the components that feeds the Agulhas Current [*Beal et al.*, 2011]. The volume of Indonesian Throughflow decreases from a mean value of ~14 Sv to ~8.5 Sv in the climate change simulation.

4. Discussion

[34] The differences in Southern Ocean circulation between the HiGEM control and climate change simulations create an interesting picture. In response to an overall 1.3° southward shift in the westerly winds, the STF moves south over steep topographic gradients in the Atlantic and Indian Sectors. In contrast there is minimal movement of most fronts within the ACC, even in the Pacific Sector where the ocean floor is relatively flat and large changes to the mean wind field are observed.

[35] It is important to note the time scale studied here. The positions of fronts shown in Figure 10a are 30-year means. Studies using satellite observations of SSH and SST have shown that there is significant inter-annual as well as seasonal variability in the location of fronts within the ACC, particularly over flat topography in the Pacific Sector [*Sallée et al.*, 2008; *Sokolov and Rintoul*, 2009]. Our result, that the mean position of most ACC fronts does not change in the climate change simulation, does not contradict these findings. Indeed, inter-annual variability of front location is also observed in HiGEM (Figure 2). What our results show is that there is little multidecadal variability in the position of most ACC fronts around the circumpolar belt and moreover that there is no large scale response in the location of these fronts to the change in the mean wind-forcing over the Southern Ocean, except in the lee of the Kerguelen Plateau.

[36] It is interesting that fronts in the Pacific Sector, where the model topography is predominantly flat, respond little to the change in mean wind field (Figures 10a, 11f and 11i). For topographic features with a short meridional length scale, turbulent eddies should diffuse the effect of local topographically induced PV gradients which influence the flow [*Thompson*, 2010]. Further, it is assumed in many studies that fronts respond more sensitively to changes in the wind field where the ocean floor is flat, away from large topographic features [*Hayward et al.*, 2008; *Howard and Prell*, 1992; *Kemp et al.*, 2010]. Typically in the HiGEM Pacific Sector, east of 260°E, meridional topographic slopes beneath jets do not exceed 2° latitude in length and 500 m in height. In contrast, throughout many other regions in the Southern Ocean mid ocean ridges span as much as 10° latitude and exceed 2 km in height. It is unclear whether these small-scale local topographic features in the model's Pacific Sector can explain why the fronts do not shift in this region during the climate change simulation. We speculate that the mean location of ACC fronts could be constrained by larger topographic features up and downstream of the front. Upstream and downstream topography has been shown to influence jets in quasi-geostrophic models [*Tansley and Marshall*, 2001]. An important question that arises from the study by *Tansley and Marshall* [2001] and warrants further investigation is how far upstream and downstream topographic features can influence fronts.

[37] The stratification of the ocean may help explain the contrasting response of different fronts in HiGEM to the change in wind-forcing. North of the ACC the water column is more stratified and the flow more baroclinic. Jets

associated with fronts in these regions are surface intensified and confined to the upper ocean (Figure 11j). These fronts, namely the STF and Agulhas front, are therefore decoupled from the bottom topography and can move more freely in response to changes in the wind-forcing. Further south, where the water column is weakly stratified, the flow becomes more barotropic. Most fronts within the ACC extend down to the ocean floor (Figures 11j–11l) and are therefore sensitive to the bottom topography and more resistant to move in response to a change in wind-forcing. The exception to this case is in the lee of the Kerguelen Plateau. Here we observe a large shift of a front within the ACC boundaries. However, consistent with our explanation, the cross section of zonal velocity shows that the front which moved at ~52°S is more baroclinic than the front at ~46°S which did not move (Figure 11k).

[38] If, as our results suggest, the baroclinicity of a front determines its sensitivity to changes in wind field, the response of fronts to the climate change forcing in HiGEM is dependent on how realistic the vertical structure of fronts is. The hydrographic sections we studied in section 3.1 compared well to HiGEM. Using the HASO compilation of hydrographic data, *Sparrow et al.* [1996] found a similar pattern to that observed in HiGEM with fronts becoming more barotropic further south, in the region they studied between 30°E and 80°E. Furthermore, neutral density cross sections from SR3 show barotropic fronts at high latitudes extending down to the ocean floor [*Rintoul and Sokolov* 2001; *Sokolov and Rintoul*, 2002], as is found here in HiGEM. These observations suggest that HiGEM performs relatively well at representing the vertical structure of fronts. Nonetheless, the results presented in this paper are from a single model and it will be interesting to investigate how these compare with similar simulations on different models.

5. Summary

[39] The behavior of Southern Ocean fronts is analyzed using output from a control and climate change simulation, each 100 model years, on the eddy permitting global climate model HiGEM. We show that SSH contours should not be used independently to approximate the position of fronts when studying their temporal variability, as this can produce misleading results. There are regions where jets exist intermittently and as the jet dissipates the SSH contour associated with the front migrate over a wide plane. Using the SSH contour method in such regions will overestimate the temporal variability. We also compare the use of SST and SSH gradients for identifying fronts. The SSH gradient method performs well in all areas of the Southern Ocean, except for the northern STF which is density compensated in some regions and can only be observed using the SST gradient method. In contrast we find that the SST gradient is a poor tool for identifying jets in the southern region of the ocean because background SST gradients are weak in the cold southern waters.

[40] The number and intensity of fronts at each longitude is set largely by the bottom topography of the Southern Ocean. The number of fronts is reduced in regions where the path of the ACC is constricted or blocked by topography, such as Drake Passage, and the intensity of fronts' increases in these regions. In contrast to results from idealized quasi-geostrophic models, we do not find a strong relationship between jet spacing and the underlying topographic gradient [*Sinha and Richards*, 1999]. Our results suggest that the positions of fronts, especially in the Pacific, may be more influenced by upstream and downstream topography. Further idealized studies following the work of *Sinha and Richards* [1999], *Tansley and Marshall* [2001] and *Thompson* [2010] are required to improve our understanding of how topography and Southern Ocean fronts interact.

[41] The maximum zonal wind stress over the Southern Ocean intensifies and shifts southward by 1.3° latitude in the climate change simulation. However, there is no net meridional shift in the path of the ACC and the transport through Drake Passage decreases from 176 to 162 Sv. The path of the ACC is also shown to contract. There is no significant meridional shift of any fronts over the Pacific Sector, where the model topography is flat, in response to the change in wind-forcing. North of the ACC, the STF and Agulhas front shift south. The southward shift of these fronts is gradual, they do not jump, and the shift occurs over steep topographic slopes. This suggests the locations of the STF and Agulhas front are not heavily constrained by topography. A localized northward shift of a front is also observed in the lee of the Kerguelen Plateau. The fronts that move are surface intensified and confined to the upper ocean and therefore less influenced by the topography below. In contrast, fronts within the ACC are more barotropic and extend down to the ocean floor. As a result these fronts will be more sensitive to the bottom topography and therefore resistant to move in response to a change in wind-forcing. The fact the fronts do not move much over flat topography in the climate change simulation but do show large seasonal variability in location, suggests a fundamental difference between the dynamics of Southern Ocean fronts over seasonal and decadal timescales.

[42] The average meridional shift of the maximum wind stress in the climate change simulation of 1.3° is relatively small compared with shifts that have been postulated, for example, at the Last Glacial Maximum [*Toggweiler et al.*, 2006]. Interestingly however, frontal shifts within the ACC are minimal in comparison to the average 1.3° shift of winds, even over regions flat topography where wind shifts are much larger. This suggests that the locations of ACC fronts are not directly controlled by the winds above. Nevertheless, it is possible, and even likely, that larger wind shifts would have a more pronounced influence on frontal positions. Future studies are underway in which the response of Southern Ocean fronts to larger winds shifts will be examined in a high resolution ocean model.

[43] **Acknowledgments.** The UK Natural Environment Research Council funded R.M.G. through a PhD studentship at the University of East Anglia. This research was carried out on the High Performance Computing Cluster supported by the Research Computing Service at the University of East Anglia. The model was developed from the Met Office Hadley Centre Model by the UK High-Resolution Modeling (HiGEM) Project and the UK Japan Climate Collaboration (UJCC). HiGEM is supported by a NERC High Resolution Climate Modeling Grant (R8/H12/123). UJCC was supported by the Foreign and Commonwealth Office Global Opportunities Fund, and jointly funded by NERC and the DECC/Defra Met Office Hadley Centre Climate Programme (GA01101). The model integrations were performed using the Japanese Earth Simulator supercomputer, supported by JAMSTEC. The work of Pier Luigi Vidale and Malcolm Roberts in leading the effort in Japan is particularly valued.

References

Bard, E., and R. E. M. Rickaby (2009), Migration of the subtropical front as a modulator of glacial climate, *Nature*, *460*(7253), 380–383, doi:10.1038/nature08189.

Beal, L. M., W. P. M. De Ruijter, A. Biastoch, R. Zahn, and SCOR/WCRP/IAPSO Working Group 136 (2011), On the role of the Agulhas system in ocean circulation and climate, *Nature*, *472*(7344), 429–436, doi:10.1038/nature09983.

Belkin, I. M., and A. L. Gordon (1996), Southern Ocean fronts from the Greenwich meridian, *J. Geophys. Res.*, *101*(C2), 3675–3696, doi:10.1029/95JC02750.

Billany, W., S. Swart, J. Hermes, and C. J. C. Reason (2010), Variability of the Southern Ocean fronts at the Greenwich Meridian, *J. Mar. Syst.*, *82*(4), 304–310, doi:10.1016/j.jmarsys.2010.06.005.

Burls, N. J., and C. J. C. Reason (2006), Sea surface temperature fronts in the midlatitude South Atlantic revealed by using microwave satellite data, *J. Geophys. Res.*, *111*, C08001, doi:10.1029/2005JC003133.

Dencausse, G., M. Arhan, and S. Speich (2011), Is there a continuous Subtropical Front south of Africa?, *J. Geophys. Res.*, *116*, C02027, doi:10.1029/2010JC006587.

De Ruijter, W. (1982), Asymptotic analysis of the Agulhas and Brazilian current systems, *J. Phys. Oceanogr.*, *12*(4), 361–373, doi:10.1175/1520-0485(1982)012<0361:AAOTAA>2.0.CO;2.

Fyfe, J. C., and O. A. Saenko (2006), Simulated changes in the extratropical Southern Hemisphere winds and currents, *Geophys. Res. Lett.*, *33*, L06701, doi:10.1029/2005GL025332.

Gent, P., and J. C. McWilliams (1990), Isopycnal mixing in ocean circulation models, *J. Phys. Oceanogr.*, *20*(1), 150–155, doi:10.1175/1520-0485(1990)020<0150:IMIOCM>2.0.CO;2.

Griffies, S. M. (1998), The Gent-McWilliams skew flux, *J. Phys. Oceanogr.*, *28*(5), 831–841, doi:10.1175/1520-0485(1998)028<0831:TGMSF>2.0.CO;2.

Hayward, B. W., et al. (2008), The effect of submerged plateaux on Pleistocene gyral circulation and sea-surface temperatures in the southwest Pacific, *Global Planet. Change*, *63*(4), 309–316, doi:10.1016/j.gloplacha.2008.07.003.

Hogg, A. M. (2010), An Antarctic Circumpolar Current driven by surface buoyancy forcing, *Geophys. Res. Lett.*, *37*, L23601, doi:10.1029/2010GL044777.

Howard, W. R., and W. L. Prell (1992), Late Quaternary surface circulation of the southern Indian Ocean and its relationship to orbital variations, *Paleoceanography*, *7*(1), 79–117, doi:10.1029/91PA02994.

James, C., M. Tomczak, I. Helmond, and L. Pender (2002), Summer and winter surveys of the Subtropical Front of the southeastern Indian Ocean 1997–1998, *J. Mar. Syst.*, *37*(1–3), 129–149, doi:10.1016/S0924-7963(02)00199-9.

Kawagata, S. (2001), Tasman Front shifts and associated paleoceanographic changes during the last 250,000 years: Foraminiferal evidence from the Lord Howe Rise, *Mar. Micropaleontol.*, *41*(3–4), 167–191, doi:10.1016/S0377-8398(00)00058-X.

Kemp, A. E. S., I. Grigorov, R. B. Pearce, and A. C. Naveira Garabato (2010), Migration of the Antarctic Polar Front through the mid-Pleistocene transition: Evidence and climatic implications, *Quat. Sci. Rev.*, *29*(17–18), 1993–2009, doi:10.1016/j.quascirev.2010.04.027.

Kostianoy, A. (2004), Fronts in the Southern Indian Ocean as inferred from satellite sea surface temperature data, *J. Mar. Syst.*, *45*(1–2), 55–73, doi:10.1016/j.jmarsys.2003.09.004.

Kushner, P. J., I. M. Held, and T. L. Delworth (2001), Southern Hemisphere atmospheric circulation response to global warming, *J. Clim.*, *14*(10), 2238–2249, doi:10.1175/1520-0442(2001)014<0001:SHACRT>2.0.CO;2.

Moore, J. K., M. R. Abbott, and J. G. Richman (1999), Location and dynamics of the Antarctic Polar Front from satellite sea surface temperature data, *J. Geophys. Res.*, *104*(C2), 3059–3073, doi:10.1029/1998JC900032.

Moore, J. K., M. R. Abbott, G. Richman, and D. M. Nelson (2000), The Southern Ocean at the Last Glacial Maximum: A strong sink for atmospheric carbon dioxide, *Global Biogeochem. Cycles*, *14*(1), 455–475, doi:10.1029/1999GB900051.

Nees, S., L. Armand, P. De Deckker, M. Labracherie, and V. Passlow (1999), A diatom and benthic foraminiferal record from the South Tasman Rise (southeastern Indian Ocean): Implications for paleoceanographic changes for the last 200,000 years, *Mar. Micropaleontol.*, *38*, 69–89, doi:10.1016/S0377-8398(99)00039-0.

Nürnberg, D., and J. Groeneveld (2006), Pleistocene variability of the Subtropical Convergence at East Tasman Plateau: Evidence from planktonic foraminiferal Mg/Ca (ODP Site 1172A), *Geochem. Geophys. Geosyst.*, *7*, Q04P11, doi:10.1029/2005GC000984.

Orsi, H., T. Whitworth, and W. D. Nowlin Jr. (1995), On the meridional extent and fronts of the Antarctic Circumpolar Current, *Deep Sea Res., Part I*, *42*(5), 641–673, doi:10.1016/0967-0637(95)00021-W.

Peeters, F. J. C., R. Acheson, G. J. Brummer, W. P. M. De Ruijter, R. R. Schneider, G. M. Ganssen, E. Ufkes, and D. Kroon (2004), Vigorous exchange between the Indian and Atlantic oceans at the end of the past five glacial periods, *Nature*, *430*(7000), 661–665, doi:10.1038/nature02785.

Rintoul, S. R., and S. Sokolov (2001), Baroclinic transport variability of the Antarctic Circumpolar Current south of Australia (WOCE repeat section SR3), *J. Geophys. Res.*, *106*(C2), 2815–2832, doi:10.1029/2000JC900107.

Roberts, M., and D. Marshall (1998), Do we require adiabatic dissipation schemes in eddy-resolving ocean models?, *J. Phys. Oceanogr.*, *28*(10), 2050–2063, doi:10.1175/1520-0485(1998)028<2050:DWRADS>2.0.CO;2.

Roberts, M. J., et al. (2009), Impact of resolution on the Tropical Pacific Circulation in a matrix of coupled models, *J. Clim.*, *22*(10), 2541–2556, doi:10.1175/2008JCLI2537.1.

Saenko, O. A., J. C. Fyfe, and M. H. England (2005), On the response of the oceanic wind-driven circulation to atmospheric CO_2 increase, *Clim. Dyn.*, *25*(4), 415–426, doi:10.1007/s00382-005-0032-5.

Sallée, J. B., K. Speer, and R. Morrow (2008), Response of the Antarctic Circumpolar Current to atmospheric variability, *J. Clim.*, *21*(12), 3020–3039, doi:10.1175/2007JCLI1702.1.

Sen Gupta, A., A. Santoso, A. S. Taschetto, C. C. Ummenhofer, J. Trevena, and M. H. England (2009), Projected changes to the Southern Hemisphere ocean and sea ice in the IPCC AR4 climate models, *J. Clim.*, *22*(11), 3047–3078, doi:10.1175/2008JCLI2827.1.

Shaffrey, L. C., et al. (2009), U.K. HiGEM: The New U.K. High-Resolution Global Environment Model—Model description and basic evaluation, *J. Clim.*, *22*(8), 1861–1896, doi:10.1175/2008JCLI2508.1.

Sikes, E. L., W. R. Howard, C. R. Samson, T. S. Mahan, L. G. Robertson, and J. K. Volkman (2009), Southern Ocean seasonal temperature and Subtropical Front movement on the South Tasman Rise in the late Quaternary, *Paleoceanography*, *24*, PA2201, doi:10.1029/2008PA001659.

Sinha, B., and K. Richards (1999), Jet structure and scaling in Southern Ocean models, *J. Phys. Oceanogr.*, *29*(6), 1143–1155, doi:10.1175/1520-0485(1999)029<1143:JSASIS>2.0.CO;2.

Sokolov, S., and S. R. Rintoul (2002), Structure of Southern Ocean fronts at 140°E, *J. Mar. Syst.*, *37*(1–3), 151–184, doi:10.1016/S0924-7963(02)00200-2.

Sokolov, S., and S. R. Rintoul (2007), Multiple jets of the Antarctic Circumpolar Current south of Australia, *J. Phys. Oceanogr.*, *37*(5), 1394–1412, doi:10.1175/JPO3111.1.

Sokolov, S., and S. R. Rintoul (2009), Circumpolar structure and distribution of the Antarctic Circumpolar Current fronts: 2. Variability and relationship to sea surface height, *J. Geophys. Res.*, *114*, C11019, doi:10.1029/2008JC005248.

Sparrow, M. D., K. J. Heywood, J. Brown, and D. P. Stevens (1996), Current structure of the south Indian Ocean, *J. Geophys. Res.*, *101*(C3), 6377–6391, doi:10.1029/95JC03750.

Spence, P., J. C. Fyfe, A. Montenegro, and A. J. Weaver (2010), Southern Ocean response to strengthening winds in an eddy-permitting global climate model, *J. Clim.*, *23*(19), 5332–5343, doi:10.1175/2010JCLI3098.1.

Tansley, C. E., and D. P. Marshall (2001), On the dynamics of wind-driven circumpolar currents, *J. Phys. Oceanogr.*, *31*(11), 3258–3273, doi:10.1175/1520-0485(2001)031<3258:OTDOWD>2.0.CO;2.

Thompson, A. F. (2010), Jet formation and evolution in baroclinic turbulence with simple topography, *J. Phys. Oceanogr.*, *40*(2), 257–278, doi:10.1175/2009JPO4218.1.

Thompson, A. F., P. H. Haynes, C. Wilson, and K. J. Richards (2010), Rapid Southern Ocean front transitions in an eddy-resolving ocean GCM, *Geophys. Res. Lett.*, *37*, L23602, doi:10.1029/2010GL045386.

Toggweiler, J. R., J. L. Russell, and S. R. Carson (2006), Midlatitude westerlies, atmospheric CO_2, and climate change during the ice ages, *Paleoceanography*, *21*, PA2005, doi:10.1029/2005PA001154.

Volkov, D. L., and V. Zlotnicki (2012), Performance of GOCE and GRACE-derived mean dynamic topographies in resolving Antarctic Circumpolar Current fronts, *Ocean Dyn.*, *62*, 893–905, doi:10.1007/s10236-012-0541-9.

Wang, Z., T. Kuhlbrodt, and M. P. Meredith (2011), On the response of the Antarctic Circumpolar Current transport to climate change in coupled climate models, *J. Geophys. Res.*, *116*, C08011, doi:10.1029/2010JC006757.

Wells, P., and H. Okada (1997), Response of nannoplankton to major changes in sea-surface temperature and movements of hydrological fronts over Site DSDP 594 (south Chatham Rise, southeastern New Zealand), during the last 130 kyr, *Mar. Micropaleontol.*, *32*(3–4), 341–363, doi:10.1016/S0377-8398(97)00025-X.